Avalanche Breakdown of pn-junctions - Simulation by Spherical Harmonics Expansion of the Boltzmann Transport Equation

Dominic Jabs and Christoph Jungemann
Chair of Electromagnetic Theory
RWTH Aachen University
52056 Aachen, Germany
Email: jabs@ithe.rwth-aaachen.de

***Abstract*—The deterministic solution of the coupled Boltzmann transport equations for electrons and holes is calculated by means of the spherical harmonics expansion method for avalanche breakdown of a pn-junction. An iteration scheme based on a splitting of the system matrix is presented, by which a stable solution of this numerically challenging problem can be obtained.**

I. Introduction

The deterministic solution of the Boltzmann transport equation (BTE) by means of the spherical harmonics expansion (SHE) is a versatile alternative to the Monte Carlo approach [1], [2]. Its application to avalanche breakdown of a pn-junction is discussed in this work. As the avalanche breakdown of a pn-junction is a bipolar phenomenon, it must be simulated by a coupled transport model for electrons and holes. A solution of the bipolar BTE with the SHE method for electrons and holes has been shown in [3], which is extended to the case of impact ionization (II), that generates secondary charge carriers. The exponential dependence of the II generation rate on the applied bias and the avalanche effect sharply degrade the stability and convergence of the problem and require an appropriate iteration scheme for solving the bipolar BTE together with the Poisson equation for the electrostatic potential.

II. Model

The stationary carrier transport in the pn-junction is described by BTEs for the distribution functions of electrons f^e and holes f^h. For electrons it reads

$$\frac{1}{\hbar}\vec{F}\cdot\nabla_{\vec{k}}f^e(\vec{r},\vec{k})+\vec{v}\cdot\nabla_{\vec{r}}f^e(\vec{r},\vec{k}) = S\left\{f^e\right\}+Q\left\{f^e,f^h\right\} \quad (1)$$

where the left-hand side terms of Eq. 1 describe the free streaming of electrons and the right-hand side is composed of the scattering term $S\left\{f^e\right\}$ for electrons and the generation term $Q\left\{f^e,f^h\right\}$, which couples the electron distribution function f^e to the hole distribution function f^h [2]. The BTE for holes is similar. If the generation terms $Q\left\{f^e,f^h\right\}$ in the BTEs for electrons and holes are neglected, the BTEs for electrons and holes decouple. In this work $Q\left\{f^e,f^h\right\}$ must be considered, because the crucial term, that causes the avalanche breakdown of the pn-junction is the generation of secondary pairs of carriers due to II from primary electrons and primary holes.

The energy dependent II scattering rate is modeled for electrons by [4]

$$S^e_{II}(\epsilon) = \begin{cases} 1.49\cdot 10^{11}\frac{1}{s}\left(\frac{\epsilon}{eV}-1.128\right)^3 & , \frac{\epsilon}{eV}\in[1.128,1.75] \\ 1.13\cdot 10^{12}\frac{1}{s}\left(\frac{\epsilon}{eV}-1.572\right)^2 & , \frac{\epsilon}{eV}>1.75 \end{cases} \quad (2)$$

and for holes by

$$S^h_{II}(\epsilon) = \begin{cases} 6\cdot 10^{10}\frac{1}{s}\left(\frac{\epsilon}{eV}-1.125\right)^6 & , \frac{\epsilon}{eV}\in[1.125,1.45] \\ 6\cdot 10^{10}\frac{1}{s}\left(\frac{\epsilon}{eV}-1.125\right)^6 & \\ +3\cdot 10^{13}\frac{1}{s}\left(\frac{\epsilon}{eV}-1.450\right)^4 & , \frac{\epsilon}{eV}>1.45 \end{cases} \quad (3)$$

These II scattering rates reproduce measured data for the inverse ionization length and the quantum yield [5]. The transition rates $S^{e,h}_{II}(\vec{k}'|\vec{k})$ for II must reproduce these II scattering rates, when the integral

$$S^{e,h}_{II}(\vec{k}) = \int S^{e,h}_{II}(\vec{k}'|\vec{k})d^3k' \quad (4)$$

is evaluated. These transition rates enter into the scattering operator $S\left\{f^e\right\}$ due to II scattering of primary particles as well as into the generation operator $Q\left\{f^e,f^h\right\}$ due to the II generation of secondary particles. One primary particle with sufficient energy can generate via II a secondary a pair of one electron and one hole. For the sake of simplicity it is assumed that the initial energy of the generated electron and hole is zero and that each particle after the II scattering process has the same energy, so that energy conservation requires

$$\epsilon'_{II} = \frac{\epsilon-\epsilon_g}{3} \ , \quad (5)$$

with the initial energy of the primary particle ϵ, the final energy ϵ'_{II} of the three particles and the energy band gap ϵ_g [5].

The scattering terms $S\left\{f^{e/h}\right\}$ include in addition to II phonon scattering [2]. Full-band models for electrons and holes are used, because the accurate description of the bands for energies up to at least 5eV is essential for the simulation of hot carriers [6]. The bandstructure models described in [2], [7], [8] satisfy this requirement and are used here. The SHE of the BTE leads to a linear system with a sparse matrix, which is solved with the iterative solver package ILUPACK [9].

II causes additional non-diagonal elements in the sparse matrix of the BTE. These elements represent the II in-scattering

978-1-4799-5288-5/14/$31.00

from high energy states into low energy states. According to Eq. 2 and Eq. 3 these terms increase with increasing energy, and therefore a small increase of the distribution function at high energies can cause a dramatic increase of the in-scattering due to II. A bias above the breakdown voltage provides a sufficiently big distribution function at high energies of electrons and holes to initialize this effect and hence the avalanche breakdown occurs. This effect makes the system unstable for biases near the breakdown voltage. Furthermore, without II the sparse matrix is a scaled M-matrix for the lowest order SHE and this property is lost, if II is included in the BTE. This numerical disadvantage of the matrix can lead to a wrong solution with partially negative distribution functions. To improve the numerical robustness of matrix $\hat{B}(\psi)$ of the BTE for a given potential ψ and to circumvent the instability for biases near the breakdown voltage, the part of the discrete BTE due to generation of secondary particles is split off.

$$\hat{B}(\psi)\vec{f} = \left(\hat{B}^{(p)}(\psi) + \hat{B}^{(s)}(\psi)\right)\vec{f} = \vec{b}(\psi) \tag{6}$$

In Eq. 6, $\hat{B}^{(p)}(\psi)$ represents the BTE matrix with free-streaming terms as well as the scattering of the primary particles, whereas $\hat{B}^{(s)}(\psi)$ covers the generation terms of secondary pairs of particles. The matrix $\hat{B}^{(p)}(\psi)$ is charge conserving, but it is no longer a scaled M-matrix for the lowest order SHE. This separation circumvents the instability for biases near the breakdown voltage, because the crucial terms for the occurrence of an avalanche breakdown, the generation of minority carriers by majority carriers, are split off into the matrix $\hat{B}^{(s)}(\psi)$. After this separation the matrix $\hat{B}^{(p)}(\psi)$ itself can not lead to a breakdown, because the generated secondary particles are missed out. In contrast to the instable equation $\hat{B}(\psi)\vec{f} = \vec{b}(\psi)$ of the complete system in the case of a bias near the avalanche breakdown, the equation $\hat{B}^{(p)}(\psi)\vec{f} = \vec{b}(\psi)$ can still be solved. To solve the complete system, an iteration of the form

$$\hat{B}^{(p)}(\psi)\vec{f}_n = \vec{b}(\psi) - \hat{B}^{(s)}(\psi)\vec{f}_{n-1} \tag{7}$$

is performed, where $-\hat{B}^{(s)}(\psi)$ and $\vec{b}(\psi)$ are non-negative. In the step n of the iteration loop the split off in-scattering terms are evaluated with the distribution function $\vec{f}_{n-1}$ of the previous iteration step $n-1$ and enter into the right-hand site of the equation. The new distribution function $\vec{f}_n$ is then determined by solving the linear equation with the remaining matrix $\hat{B}^{(p)}(\psi)$ without secondary carriers and the updated right-hand side.

For the breakdown simulation, first a standard Gummel-type iteration loop of just $\hat{B}^{(p)}(\psi)\vec{f} = \vec{b}(\psi)$ with the Poisson equation (PE) is performed, that yields an initial solution for the densities of both carriers and for the electrostatic potential, which is used as a starting potential for the iteration scheme in Eq. 7. For a bias below the breakdown voltage this loop converges, because the charge generation by II during the iteration is not sufficient to start the avalanche breakdown and limited terminal currents are generated (Fig. 1). For a bias above the breakdown voltage this loop does not converge and the terminal currents increase exponentially (Fig. 1). Hence in the case of a bias above the breakdown the iteration loop (Eq. 7) does not converge without updating the matrices $\hat{B}^{(p)}(\psi')$ and $\hat{B}^{(s)}(\psi')$ with respect to the changed potential ψ', since the change in potential lowers the number of hot

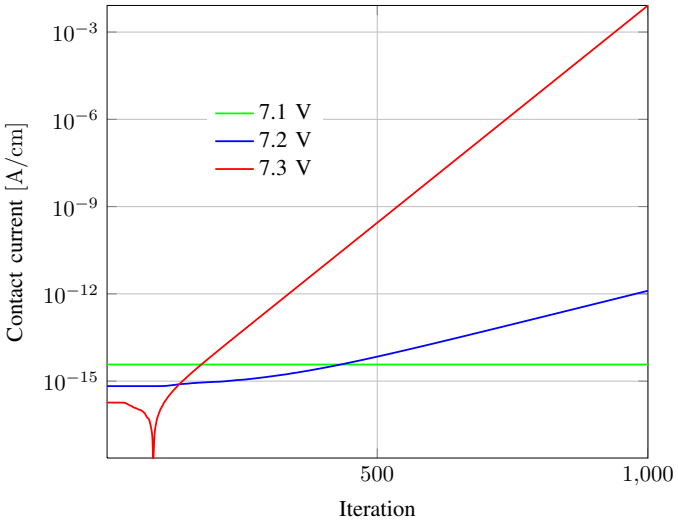

Fig. 1. Terminal currents for different biases: 7.1V is below the breakdown voltage, whereas 7.2V and 7.3V are above the breakdown voltage.

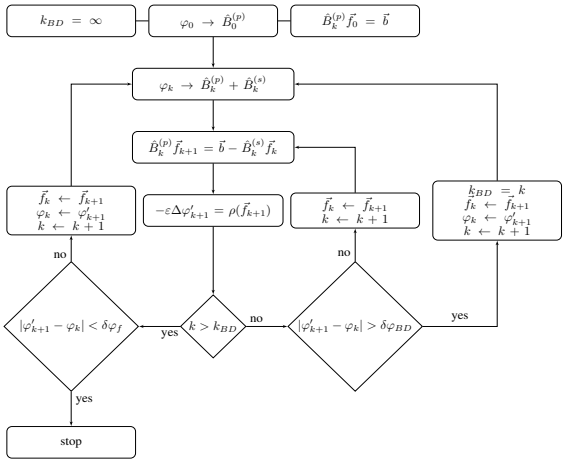

Fig. 2. Flow diagram of the algorithm of the simulation

carriers and thus II generation.

The convergence problem can be avoided by updating the potential at every iteration of Eq. 7, but this is very CPU intensive, because this requires to calculate the incomplete LU decomposition for preconditioning anew. A faster algorithm for treating the case of a bias above the breakdown voltage is to perform the iteration (Eq. 7) for a fixed initial potential until the resulting change in the potential would be above a certain threshold between 1mV and 100mV, and to only rebuild the matrices anew when this threshold is reached. This Gummel-type iteration of BTE and PE with an update of the matrices converges (Fig. 2).

III. Simulation Results

In Fig. 3, the changes in the potential during the iteration (Eq. 7) are shown with and without updating $\hat{B}(\psi)$ and in the beginning the changes in the potential are very similar. The change in the potential first increases due to the charge built-up in the junction and then decreases due to the reduction in generation of secondary particles by II.

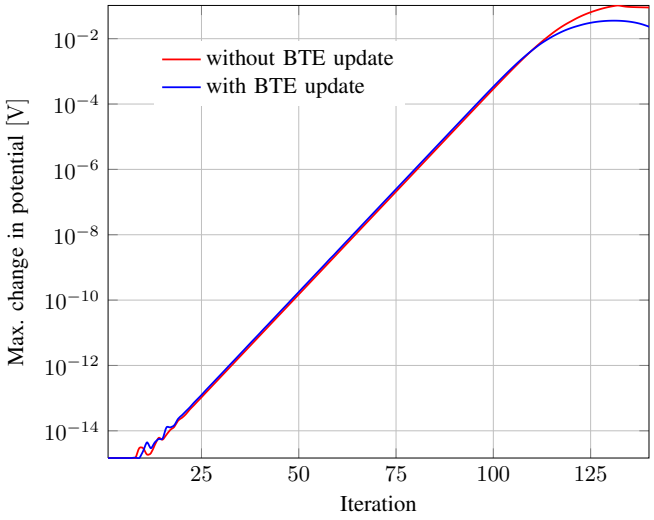

Fig. 3. Maximum change in potential during the iteration process at 8.5V

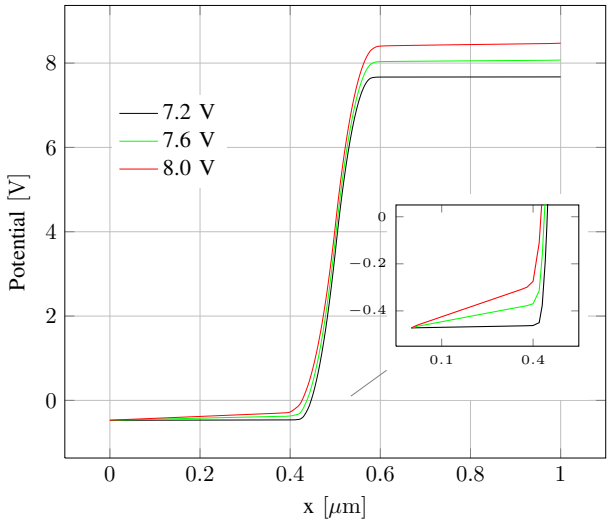

Fig. 4. Potential profile above the breakdown voltage

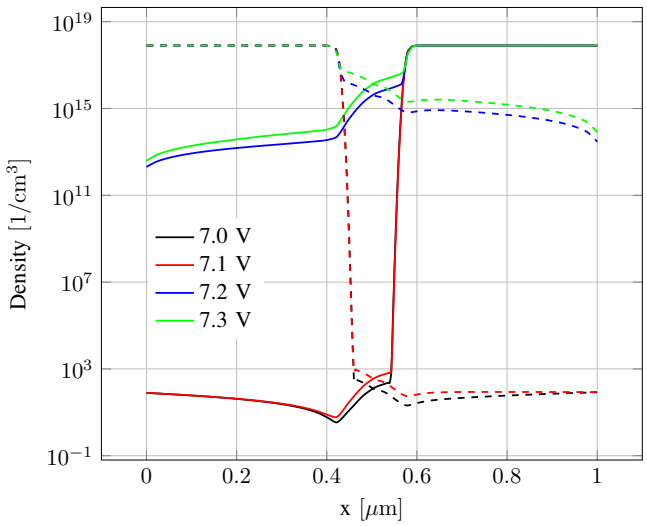

Fig. 5. Densities for electrons (solid lines) and holes (dashed lines) at biases close to the breakdown voltage

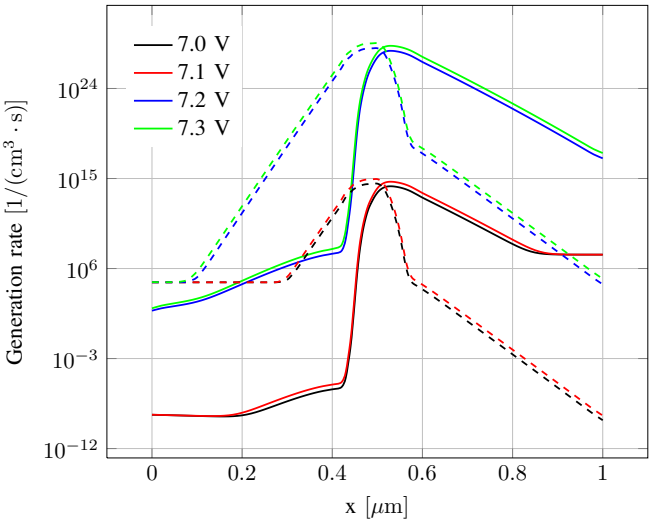

Fig. 6. Generation rates due to impact ionization for electrons (solid lines) and holes (dashed lines) at biases close to the breakdown voltage

How the increase of the charges in the junction changes the potential profile is visualized in Fig. 4. The correction in the potential profile is larger for a higher bias. The increased potential drop in the quasi-neutral regions due to the increased current limits the increase of the potential drop in the space charge region, where the particles gain the energy for II. Since the II scattering rate depends on energy (Eqs. 2-3), this limits in turn the increase in current. This self-stabilizing effect permits to get a converged solution at breakdown.

Fig. 5 shows the densities of electrons and holes for two bias points below the breakdown voltage and two above the breakdown voltage. Fig. 6 shows the corresponding II generation rates for secondary particles. The salient difference in the densities and the generation rates for biases barely below and above the breakdown voltage is illustrated in Fig. 5 and Fig. 6. Impact ionization generates carriers below the breakdown voltage as well as above, but the value of the generation rate is by orders of magnitude larger for a bias above the breakdown voltage. For a bias below the breakdown voltage the charge of these minorities compared to the charge of the majorities is not sufficient to have a notable influence on the potential.

In Fig. 7 the energy distribution functions, that are the distribution functions multiplied by the density of states, of electrons and holes are shown as functions of the energy at the maximum position of the II generation rate and at the beginning and end of the space charge region. The noticeable values of the energy distribution functions at high energies in the II generation region close to the junction clarify that the simulation of an energy interval from 0eV to at least 5eV should be considered.

The current voltage characteristic can be obtained by this method (Fig. 8). The determination of the bias points close to the breakdown voltage needs the most computational effort, as the slopes in Fig. 1 and Fig. 3 for these bias points are small and therefore many iterations are needed in the inner loop of the iteration scheme (Fig. 2).

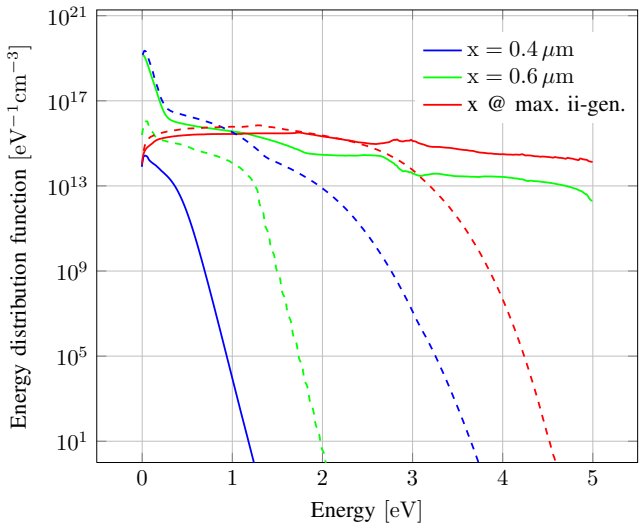

Fig. 7. Energy distribution functions of electrons (solid line) and holes (dashed line) at different positions in the pn-junction for 7.2V

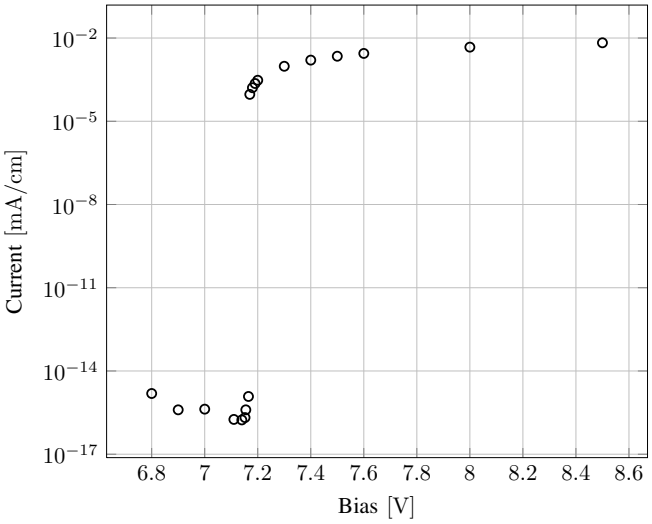

Fig. 8. Resulting current-voltage characteristic of the pn-junction

IV. Conclusion

We have presented the first simulations of the avalanche breakdown in a pn-junction by solving the bipolar BTE with the deterministic SHE approach. Compared to the Monte-Carlo method the SHE approach has the advantage that a stationary state is obtained directly, that the distribution functions are available over many orders of magnitude as required by the simulation of degradation, and that small-signal and noise analyses are possible. The presented methods are not restricted to pn-junctions and can also be used in the case of more complex devices (e.g. power devices).

Acknowledgment

The authors gratefully acknowledge financial support by the German Federal Ministry for Economic Affairs and Energy under contract number FKZ03ET6003A-I (DriveBattery2015).

References

[1] A. Gnudi, D. Ventura, G. Baccarani, and F. Odeh, "Two-dimensional MOSFET simulation by means of a multidimensional spherical harmonics expansion of the Boltzmann transport equation," *Solid–State Electron.*, vol. 36, no. 4, pp. 575 – 581, 1993.

[2] S.-M. Hong, A. T. Pham, and C. Jungemann, *Deterministic solvers for the Boltzmann transport equation*, ser. Computational Microelectronics, S. Selberherr, Ed. Wien, New York: Springer, 2011.

[3] K. Rupp, C. Jungemann, M. Bina, A. Jüngel, and T. Grasser, "Bipolar spherical harmonics expansion of the Boltzmann transport equation," in *Proc. SISPAD*, 2012, pp. 19–22.

[4] R. Thoma, H. J. Peifer, W. L. Engl, W. Quade, R. Brunetti, and C. Jacoboni, "An improved impact–ionization model for high–energy electron transport in Si with Monte Carlo simulation," *J. Appl. Phys.*, vol. 69, pp. 2300–2311, 1991.

[5] C. Jungemann and B. Meinerzhagen, *Hierarchical Device Simulation: The Monte-Carlo Perspective*, ser. Computational Microelectronics. Wien, New York: Springer, 2003.

[6] A. Abramo, L. Baudry, R. Brunetti, R. Castagne, M. Charef, F. Dessenne, P. Dollfus, R. Dutton, W. Engl, R. Fauquembergue, C. Fiegna, M. Fischetti, S. Galdin, N. Goldsman, M. Hackel, C. Hamaguchi, K. Hess, K. Hennacy, P. Hesto, J. Higman, T. Iizuka, C. Jungemann, Y. Kamakura, H. Kosina, T. Kunikiyo, S. Laux, H. Lin, C. Maziar, H. Mizuno, H. Peifer, S. Ramaswamy, N. Sano, P. Scrobohaci, S. Selberherr, M. Takenaka, T. wei Tang, K. Taniguchi, J. Thobel, R. Thoma, K. Tomizawa, M. Tomizawa, T. Vogelsang, S.-L. Wang, X. Wang, C.-S. Yao, P. Yoder, and A. Yoshii, "A comparison of numerical solutions of the boltzmann transport equation for high-energy electron transport silicon," *Electron Devices, IEEE Transactions on*, vol. 41, no. 9, pp. 1646 –1654, sept. 1994.

[7] M. C. Vecchi and M. Rudan, "Modeling electron and hole transport with full-band structure effects by means of the spherical-harmonics expansion of the BTE," *Electron Devices, IEEE Transactions on*, vol. 45, no. 1, pp. 230–238, 1998.

[8] S. Jin, S.-M. Hong, and C. Jungemann, "An efficient approach to include full-band effects in deterministic boltzmann equation solver based on high-order spherical harmonics expansion," *Electron Devices, IEEE Transactions on*, vol. 58, no. 5, pp. 1287 –1294, may 2011.

[9] M. Bollhöfer and Y. Saad, "Multilevel preconditioners constructed from inverse–based ILUs," *SIAM J. Sci. Comput.*, vol. 27, no. 5, pp. 1627–1650, 2006.